Stellar magnetic cycles observed and simulated

A. Strugarek[1,2], P. Beaudoin[1], P. Charbonneau[1], A.S. Brun[2] & J.-D. do Nascimento Jr.[3,4]

[1]*Département de physique, Université de Montréal, C.P. 6128 Succ. Centre-Ville, Montréal, QC H3C-3J7, Canada*
[2]*Laboratoire AIM Paris-Saclay, CEA/Irfu Université Paris-Diderot CNRS/INSU, F-91191 Gif-sur-Yvette*
[3]*Harvard-Smithsonian Center for Astrophysics, Cambridge, Massachusetts 02138, USA*
[4]*Univ. Federal do Rio Grande do Norte, UFRN, Dep. de Física Teórica DFTE, CP 1641, 59072-970, Natal, RN, Brazil*

The magnetic field of solar-type stars influences their evolution, shapes their astrosphere, and impacts their orbiting planets. They are observed to regularly cycle over decadal periods (11 years in the case of our Sun) and were reported to have a complex dependency upon stellar rotation[1]. This cyclic behavior takes its roots into the dynamo mechanism(s) sustaining stellar magnetic fields, which depend on the large-scale flows as well as the properties of convective turbulence inside the star. However, the detailed interplay between rotation, convection and magnetism that leads to cyclic magnetic fields still resists our physical understanding. Here we report on a set of turbulent global numerical simulations that exhibit magnetic cycles varying systematically with rotation and luminosity. We find that the magnetic cycle period is inversely proportional to the Rossby number, in opposition with previous estimates based on linear mean-field dynamo theory. Furthermore, this trend is shown to be compatible with the cycle period of the sun and other solar-type stars. Our results suggest that the magnetic cycle of these stars can be attributed to a non-linear dynamo process ubiquitously occurring in their turbulent convection zone, with the stellar luminosity and rotation rate jointly controlling the cycle period.

Ongoing searches for exoplanets have spurred renewed interest in the characterization of stellar activity, and its ultimate dynamo origin. The wealth of new observational data now makes it possible to determine absolute luminosities via accurate parallax measurements, rotation through Doppler measurements and precision photometry, stellar differential rotation through photometry and asteroseismic sounding, and the large-scale spatial structure of stellar photospheric magnetic fields through Zeeman-Doppler imaging. These data represent a crucial complement to stellar activity measurements available from the long term monitoring programs at the Mt Wilson and Lowell Observatories[2,3]. Of particular interest are variations of stellar cycle amplitudes and periods as a function of fundamental stellar parameters such as mass, luminosity, and rotation. The physical picture emerging from these joint datasets turns out to be more complex than suggested by prior interpretation of stellar cycle data through mean-field dynamo theory[1,4,5].

In parallel to these renewed observational efforts, numerous global magnetohydrodynamical (MHD) simulations of solar convection have succeeded in producing large-scale magnetic fields over the past decades[6-11], in some cases generating regular, solar-like cyclic magnetic polarity reversals[12-17]. These

simulations also generate large-scale flows such as differential rotation in a dynamically consistent manner, and thus offer unique test beds for the physical interpretation of stellar magnetic cycle observations.

We report here on a set of such global MHD simulations carried out with the EULAG code[18,20], using a fixed background stellar structure but covering a factor of 2 in rotation rates and 3 in convective luminosity. The simulated domain consists in a global (i.e. spherical) stellar convection zone with a solar-like aspect ratio ($R_{bottom} \sim 0.7\ R_{top}$) covering 3.22 density scale-heights. All simulations in the set generate some tantalizingly solar-like features, including: (i) an accumulation of a strong, large-scale axisymmetric magnetic field at the bottom of the convection zone, (ii) regular polarity reversals on a decadal time-scale, reasonably well synchronized across hemispheres, and (iii) an equatorial propagation of the large-scale magnetic field (see Figure 1), (iv) a solar-like differential rotation (fast equator, slow poles; with one simulation standing close to the transition to anti-solar rotation). The more obvious non-solar features are the concentration of toroidal field bands at mid- rather than low-latitudes, and an irregularly alternating pattern of symmetric and anti-symmetric equatorial parity. This is clearly apparent in panel D in Figure 1 where periods of symmetrical and anti-symmetrical states follow up one another. Such parity drifts are understood to reflect the interactions between the two families of dynamo symmetry[19-21], which couple in the non-linear regime.

The magnetic cycle trends in our set of simulations are displayed in Figure 2 (blue circles with error-bars). Two main trends are unambiguously identified. First, the magnetic cycle period is found to decrease proportionally to the rotation rate when the convective luminosity is held constant (red squares in panel A). Second, the cycle period also decreases with increasing convective luminosity ($P_{cyc} \propto L_{bc}^{-0.8}$) at constant rotation rate (red squares in panel B). In each panel, the position of the Sun is labeled by the standard solar symbol ($\odot$) in magenta. The secondary solar cycle of 2 years identified through helioseismology[22-24] is also shown by a smaller symbol. The luminosity dependency is scaled out in panel C. Our simulation results then collapse onto a single trend with rotation rate that is very close to matching the Sun. This result is quite encouraging, as the aspect ratio of the convection zones simulated here is very close to solar.

We further compare our results to the growing sample of observed magnetic cycles of distant stars. Two samples of stars are shown in Figure 2, observed with Mt Wilson spectrophotometers (BV sample, cyan stars)[1,5,25] and with the HARPS spectrograph (L11 sample, orange diamonds)[26,27]. We reanalyzed part of the latter sample due to significant error bars in the originally reported cycle periods. The original sample is shown in transparent diamonds for reference, and the solid orange diamonds label robust cycle periods found after re-analysis. As the luminosity of the two samples was not reported in the literature, we calculated it using Hipparcos parallaxes[28], V magnitude, and a standard bolometric correction[29]. The errors on the Hipparcos parallaxes translate into errors in luminosity that are less than 10% for most of the stars in the two samples. The samples are composed of stars with very different spectral types, and consequently very different convection zone aspect ratios and luminosities. Some stars also exhibit two different cycles periods, in which cases both periods are plotted in Figure 2 and linked by a dashed line.

Several "activity branches" have historically been defined in these samples[1,30,31], the two primary branches both showing a positive correlation between cycle and rotation periods. Our simulation results point to a different interpretation, in which the cycle period is instead *inversely* proportional to the rotation period. This is due in part to the strong dependence of the cycle period on the convective luminosity, as emerging from our simulation set, which was not taken into account in earlier analyses of these stellar data. On panel C in Figure 2 we plot the observed magnetic cycle period multiplied by a corrective proportionality factor deduced from our simulations, so as to remove the inferred stellar luminosity dependency. The corrected cycle periods of the observed stars then also align on a trend inversely proportional to the stellar rotation period, as suggested by our numerical simulations. We furthermore highlight in magenta four stars that are likely to possess a convection zone of depth similar to the sun's. Three of the four identified stars align very well on the trend suggested by our numerical simulations. The sample of stars still shows a large spread around this trend, which is likely due to (i) the varying aspect ratio of the convection zone of the stars in the samples and (ii) the existence of multiple cycle periods for several stars.

The interpretation of observed cycle period variations with stellar parameters have most often been based on kinematic dynamo models formulated through mean-field theory[1,4]. The two key ingredients in such models are differential rotation and cyclonic turbulence, both resulting ultimately from the action of the Coriolis force on thermally driven convection. In this context, the governing parameter is the Rossby number (R_o), which measures the dimensionless ratio of the non-linear advection to the Coriolis force (see also supplementary materials). Mean field dynamo theory thus suggests a direct relationship between cycle properties and the Rossby number. This expectation is realized in our set of simulations, as shown in Figure 3. The cycle period is found to scale as R_o^{-1}, in contrast to dimensional inferences from kinematic, linear mean-field dynamo[32], which predicts cycle periods varying instead as R_o^{+1}.

This is of course not particularly surprising in itself, as our numerical simulations operate in the nonlinearly saturated regime in which the magnetic force alters the balance establishing the large-scale flows (here the differential rotation and meridional circulation). In the panel B of Figure 3 we show the systematic acceleration of the differential rotation (red threads propagating towards the equator) that modifies the electromotive force (white contours) to trigger the polarity inversion of the mean azimuthal magnetic field (grey contours). The amplitude of these fluctuations of the differential rotation is small (of the order of a percent), similarly to the observed torsional oscillations on the Sun. A detailed analysis of our simulations reveals that the torque applied by the large-scale magnetic field controls these modulations. Furthermore, the magnetic cycle period decreases when the amplitude of the differential rotation modulation increases, highlighting the key role of the non-linear feedback of the Lorentz force on the large-scale differential rotation in driving polarity reversals and setting the cycle period. Such effects have no counterparts in classical kinematic dynamo theory, within which magnetic cycles are ascribed to a dynamo wave materializing under a steady differential rotation.

Recent stellar data is gradually filling the gap between what were traditionally considered to be two distinct branches in the rotation-cycle period diagram for solar-type stars[1,5] (see left panel in Figure 2). This left the Sun inconveniently lying in

between, forcing to conjecture that it just happens to be in a transition state between these two branches. Although restricted in the stellar parameter range they span, our simulation results suggest a single trend of cycle period with rotational influence -as quantified by the Rossby number- that can accommodate both the sun and extant stellar data within a single dynamo branch. The scatter about the mean relationship observed between cycle period and rotation rate is then attributed to the sensitive dependence of the cycle period on luminosity, and perhaps other structural factor such as the exact depth of the convection zone. Different tendencies at larger Rossby number may also be expected, and require further inquires. Taken at face value, these considerations would reinstate the Sun to the status of an ordinary solar-type star, and true Rosetta stone of stellar astrophysics.

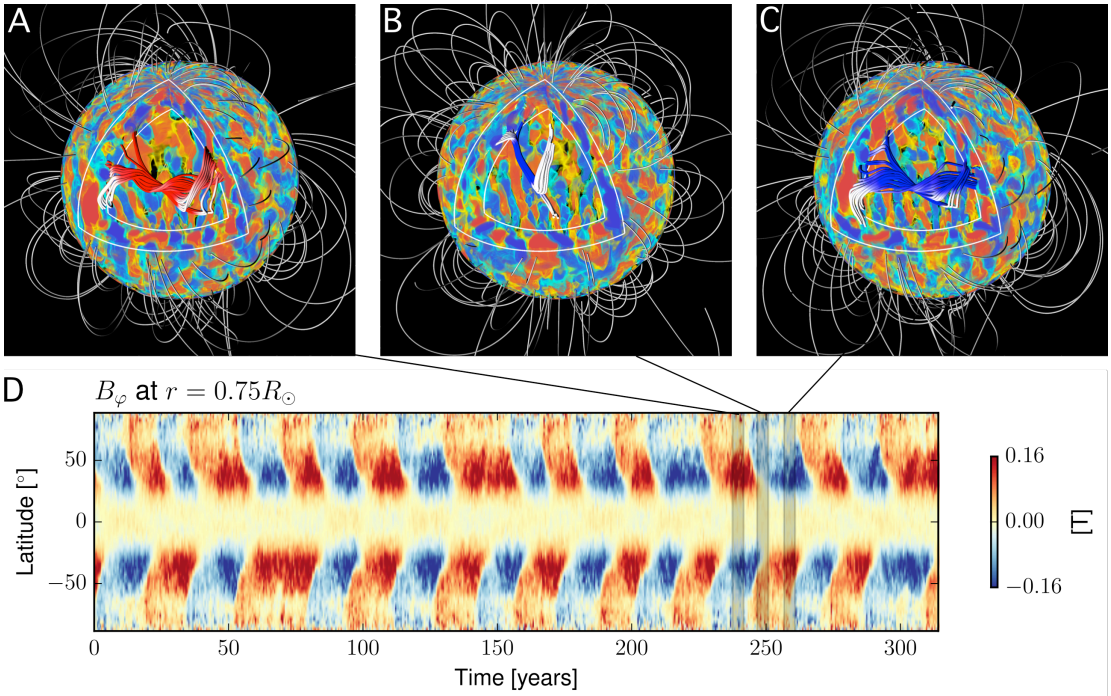

Figure 1 | A regular magnetic cycle. (A-C) Snapshots of a representative three-dimensional simulation of a regular non-linear magnetic cycle. Red (positive) and blue (negative) volumes represent the radial velocity (v_r) of the convective flow. A half sector of the spherical shell has been cut out to display the large scale magnetic field lines buried in the convection zone (the red/blue coloring of the magnetic tubes labels positive/negative azimuthal magnetic field). These field lines trace the large-scale magnetic field averaged over 50 rotation periods. In panel B the magnetic field is 4 times weaker than in panels A and C, making the deeply seated magnetic field lines less meaningful. The magnetic field lines outside of the simulation domain (grey tubes) are derived using a standard potential field extrapolation. (D) Azimuthal average of the azimuthal component of the magnetic field as a function of latitude and time at depth r=0.75 $R_\star$.

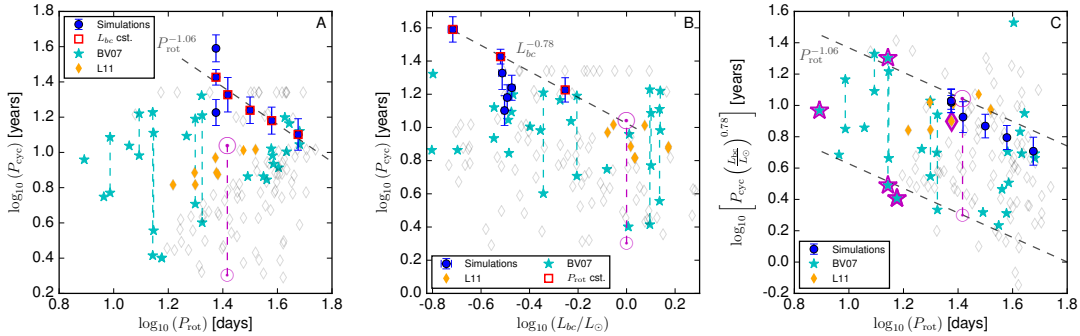

Figure 2 | Systematic trends of the cycle period. The cycle half-period (11 and 2 years for the Sun) are plotted against rotation period (A) and stellar luminosity (B) for our set of simulations (blue circles) and two observed samples of stars (cyan stars and orange diamonds) [1,5]. The dependence of the cycle period upon the stellar convective luminosity observed in our set of simulations is factored out on panel C, which collapses our simulations on a single scaling law with the rotation period, consistent with observational data after applying the same luminosity-based correction.

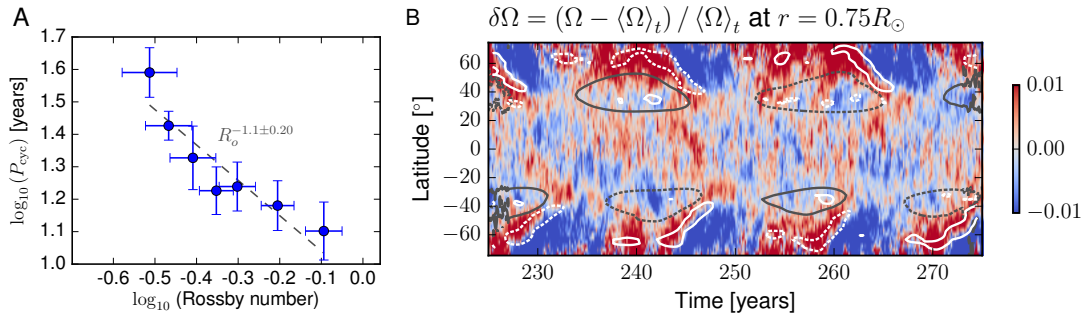

Figure 3 | Interpretation of the convective dynamo (A) Magnetic cycle period as a function of the local Rossby number deep in the convection zone in our set of simulations. The fitted scaling law indicated by the dashed grey line is compatible with a simple $P_{cyc} \propto R_o^{-1}$ dependence. (B) Relative variation (compared to the temporal average) of the differential rotation as a function of latitude and time at depth r=0.75 $R_\star$. The iso-contours of the mean azimuthal magnetic field at ±0.1 Tesla are shown in grey (see also Figure 1). The contribution of shearing by differential rotation to the mean electro-motive force is shown as white contours. For both sets of contours, solid lines correspond to positive values and dashed lines to negative values. The polarity inversion (i.e. the destruction of the azimuthal magnetic field) is hence driven by the regular non-linear acceleration of the differential rotation (red regions at mid-to-high latitudes).

Online Content Methods, along with any additional Extended Data display items and Source Data, are available in the online version of the paper; references unique to these sections appear only in the online paper.

References

1. Saar, S. H. & Brandenburg, A. Time Evolution of the Magnetic Activity Cycle Period. II. Results for an Expanded Stellar Sample. *apj* **524,** 295–310 (1999).

2. Baliunas, S. L. *et al.* Chromospheric variations in main-sequence stars. *apj* **438,** 269–287 (1995).
3. Hall, J. C., Lockwood, G. W. & Skiff, B. A. The Activity and Variability of the Sun and Sun-like Stars. I. Synoptic Ca II H and K Observations. *The Astronomical Journal* **133,** 862–881 (2007).
4. Noyes, R. W., Weiss, N. O. & Vaughan, A. H. The relation between stellar rotation rate and activity cycle periods. *apj* **287,** 769–773 (1984).
5. Bohm Vitense, E. Chromospheric Activity in G and K Main-Sequence Stars, and What It Tells Us about Stellar Dynamos. *apj* **657,** 486–493 (2007).
6. Brown, B. P., Miesch, M. S., Browning, M. K., Brun, A. S. & Toomre, J. Magnetic Cycles in a Convective Dynamo Simulation of a Young Solar-type Star. *apj* **731,** 69 (2011).
7. Käpylä, P. J., Mantere, M. J., Cole, E., Warnecke, J. & Brandenburg, A. Effects of Enhanced Stratification on Equatorward Dynamo Wave Propagation. *apj* **778,** 41 (2013).
8. Masada, Y., Yamada, K. & Kageyama, A. Effects of Penetrative Convection on Solar Dynamo. *apj* **778,** 11 (2013).
9. Nelson, N. J., Brown, B. P., Brun, A. S., Miesch, M. S. & Toomre, J. Magnetic Wreaths and Cycles in Convective Dynamos. *apj* **762,** 73 (2013).
10. Fan, Y. & Fang, F. A Simulation of Convective Dynamo in the Solar Convective Envelope: Maintenance of the Solar-like Differential Rotation and Emerging Flux. *apj* **789,** 35 (2014).
11. Hotta, H., Rempel, M. & Yokoyama, T. Large-scale magnetic fields at high Reynolds numbers in magnetohydrodynamic simulations. *Science* **351,** 1427–1430 (2016).
12. Ghizaru, M., Charbonneau, P. & Smolarkiewicz, P. K. Magnetic Cycles in Global Large-eddy Simulations of Solar Convection. *apjl* **715,** L133–L137 (2010).
13. Passos, D. & Charbonneau, P. Characteristics of magnetic solar-like cycles in a 3D MHD simulation of solar convection. *aap* **568,** 113 (2014).
14. Augustson, K., Brun, A. S., Miesch, M. & Toomre, J. Grand Minima and Equatorward Propagation in a Cycling Stellar Convective Dynamo. *apj* **809,** 149 (2015).
15. Simitev, R. D., Kosovichev, A. G. & Busse, F. H. Dynamo Effects Near the Transition from Solar to Anti-Solar Differential Rotation. *apj* **810,** 80 (2015).
16. Duarte, L. D. V., Wicht, J., Browning, M. K. & Gastine, T. Helicity inversion in spherical convection as a means for equatorward dynamo wave propagation. *mnras* **456,** 1708–1722 (2016).
17. Guerrero, G., Smolarkiewicz, P. K., de Gouveia Dal Pino, E. M., Kosovichev, A. G. & Mansour, N. N. On the Role of Tachoclines in Solar and Stellar Dynamos. *apj* **819,** 104 (2016).
18. Prusa, J. M., Smolarkiewicz, P. K. & Wyszogrodzki, A. A. EULAG, a computational model for multiscale flows. *Computers & Fluids* **37,** 1193–1207 (2008).
19. Bullard, E. & Gellman, H. Homogeneous Dynamos and Terrestrial Magnetism. *Philos. Trans. R. Soc. London, Ser. A* **247,** 213–278 (1954).
20. Roberts, P. H. & Stix, M. Ac-Effect Dynamos, by the Buliard-Geflman Formalism. *aap* **18,** 453 (1972).
21. Gubbins, D. & Zhang, K. Symmetry properties of the dynamo equations for palaeomagnetism and geomagnetism. *Physics of the Earth and Planetary*

Interiors **75,** 225–241 (1993).
22. Fletcher, S. T. *et al.* A Seismic Signature of a Second Dynamo? *apjl* **718,** L19–L22 (2010).
23. Simoniello, R. *et al.* The Quasi-biennial Periodicity as a Window on the Solar Magnetic Dynamo Configuration. *apj* **765,** 100 (2013).
24. Ulrich, R. K. & Tran, T. The Global Solar Magnetic Field—Identification of Traveling, Long-lived Ripples. *apj* **768,** 189 (2013).
25. Noyes, R. W., Hartmann, L. W., Baliunas, S. L., Duncan, D. K. & Vaughan, A. H. Rotation, convection, and magnetic activity in lower main-sequence stars. *apj* **279,** 763–777 (1984).
26. Mayor, M. *et al.* Setting New Standards with HARPS. *The Messenger (ISSN0722-6691)* **114,** 20–24 (2003).
27. Lovis, C. *et al.* The HARPS search for southern extra-solar planets. XXXI. Magnetic activity cycles in solar-type stars: statistics and impact on precise radial velocities. *to appear in ApJ* **1107,** arXiv:1107.5325 (2011).
28. van Leeuwen, F. Hipparcos, the New Reduction of the Raw Data. *Astrophysics and Space Science Library* **350,** (2007).
29. Torres, G. On the Use of Empirical Bolometric Corrections for Stars. *The Astronomical Journal* **140,** 1158–1162 (2010).
30. do Nascimento, J.-D. J., Saar, S. H. & Anthony, F. A New Light on the Relation Between Rotation Periods and Cycle Lengths of Stellar Activity. *18th Cambridge Workshop on Cool Stars, Stellar Systems, and the Sun* **18,** 59–64 (2015).
31. Metcalfe, T. S., Egeland, R. & van Saders, J. Stellar Evidence That the Solar Dynamo May Be in Transition. *apjl* **826,** L2 (2016).
32. Noyes, R. W., Weiss, N. O. & Vaughan, A. H. The relation between stellar rotation rate and activity cycle periods. *apj* **287,** 769–773 (1984).
33. Lipps, F. B. & Hemler, R. S. A Scale Analysis of Deep Moist Convection and Some Related Numerical Calculations. *J. Atmospheric Sci.* **39,** 2192–2210 (1982).
34. Braginsky, S. I. & Roberts, P. H. Equations governing convection in earth's core and the geodynamo. *gafd* **79,** 1–97 (1995).
35. Lantz, S. R. & Fan, Y. Anelastic Magnetohydrodynamic Equations for Modeling Solar and Stellar Convection Zones. *apjs* **121,** 247–264 (1999).
36. Smolarkiewicz, P. K. & Charbonneau, P. EULAG, a computational model for multiscale flows: An MHD extension. *J. Comp. Phys.* **236,** 608–623 (2013).
37. Domaradzki, J. A., Xiao, Z. & Smolarkiewicz, P. K. Effective eddy viscosities in implicit large eddy simulations of turbulent flows. *PoF* **15,** 3890–3893 (2003).
38. Strugarek, A. *et al.* Modeling turbulent stellar convection zones: Sub-grid scales effects. *adv* **58,** 1538–1553 (2016).
39. Jones, C. A. *et al.* Anelastic convection-driven dynamo benchmarks. *Icarus* **216,** 120–135 (2011).
40. Prusa, J. M. & Smolarkiewicz, P. K. An all-scale anelastic model for geophysical flows: dynamic grid deformation. *J. Comp. Phys.* **190,** 601–622 (2003).
41. Featherstone, N. A. & Miesch, M. S. Meridional Circulation in Solar and Stellar Convection Zones. *apj* **804,** 67 (2015).
42. Cossette, J.-F., Charbonneau, P., Smolarkiewicz, P. K. & Rast, M. P. Magnetically-modulated heat transport in global simulations of solar magneto-

convection. *Submitted to ApJ* (2016).
43. Collaboration Gaia. VizieR Online Data Catalog: Gaia DR1 (Gaia Collaboration, 2016). *VizieR Online Data Catalog* **1337,** (2016).
44. Porto de Mello, G. F. & da Silva, L. HR 6060: The Closest Ever Solar Twin? *apj* **482,** L89–L92 (1997).
45. Hardorp, J. The sun among the stars. I - A search for solar spectral analogs. *aap* **63,** 383–390 (1978).

Acknowledgements We thank P. Smolarkiewicz for his help and advice using the EULAG code and J.F. Cossette for discussions about the modeling of convection inside stars. A.S. acknowledges funding from the Canadian Institute for Theoretical Astrophysics (CITA National fellow). The authors acknowledge support from Canada's Natural Sciences and Engineering Research Council. This work was also partially supported by the INSU/PNST, the ANR 2011 Blanc Toupies, and the ERC Grant STARS2 207430. This research made use of the Vizier (http://vizier.u-strasbg.fr/cgi-bin/VizieR) and SIMBAD (http://simbad.u-strasbg.fr/simbad/sim-fid) databases (operated at CDS, Strasbourg, France), and of the Astroquery package.

Author Contributions A.S. conducted and analyzed the numerical simulations presented in this work using Compute-Canada/Calcul-Québec computing infrastructures. A.S. and J.-D. do Nascimento Jr. computed the luminosity of the samples of stars presented in this work. J.-D. do Nascimento Jr. re-analyzed the second sample of stars to identify robust cycle periods displayed as plain orange diamonds. P. Beaudoin and P. Charbonneau participated in the detailed analysis and physical interpretation of the results. A.S. Brun helped designing the models and participated in the physical interpretation of the results. All authors discussed and commented on the manuscript.

Author Information Reprints and permissions information is available at www.nature.com/reprints. The authors declare no competing financial interests. Readers are welcome to comment on the online version of the paper. Correspondence and requests for materials should be addressed to A.S. (strugarek@astro.umontreal.ca).

METHODS

The EULAG code. The Eulerian-Lagrangian (EULAG) code solves the anelastic form of the MHD equations[33-35] without explicit dissipative terms. Numerical stability is enforced through the dissipation provided by the underlying advection algorithm[36], which effectively acts as an implicit subgrid model[37,38]. In the work presented here the domain consist of a convective layer with no underlying stable zone[38,39]. The bottom spherical boundary is a perfectly conducting stress-free wall, which acts as a deep strongly stratified conducting layer. The top of the simulation domain is also impenetrable and stress-free, and the magnetic field is forced to be radial so as to mimic the connection to a stellar chromospheric layer. Convective motions are driven through a volumetric heating/cooling driving the thermal structure towards a mildly superadiabatic ambient stratification[36,38,40]. Under such a thermal forcing setup, the transport of heat (the convective luminosity) associated to convective motions is an output of the simulation and is computed *a posteriori*.

Set of numerical simulations. We display a summary figure of the properties of three representative numerical simulations of our study in Figures 4, 5 and 6. Figure 4 summarized our reference simulation shown in Figure 1. Figure 5 shows a case with faster rotation, and Figure 6 a case with faster rotation and larger convective luminosity. The layout of the three figures is the same and is as follows. The differential rotation (panel A) and meridional circulation (panel B) are averaged over longitude and over multiple magnetic cycle. The three cases show a solar-like differential rotation pattern (slow poles, fast equator). The differential rotation strengthens when the rotation rate increases (from Figure 4 to Figure 5) and when the convective luminosity increases (from Figure 5 to Figure 6). In the latter case, it is interesting to note that the rotation profile weakens at the equator when the luminosity increases, but more strongly decreases at the pole which makes the latitudinal contrast of the differential rotation increase with the stellar luminosity. The meridional flow evolves accordingly[41] and remains mostly multi-cellular at the equator and mono-cellular at higher latitude. The convective flows are shown on panel C by the representation of the radial velocity on a Mollweide projection on the sphere at depth $r=0.75\ R_\star$. In Figure 5 and 6 the "banana cells" (elongated cells in the polar direction which exist in the equatorial region, outside of the tangent cylinder) appear more clearly than in Figure 4, which is expected as these models rotate faster. The time-latitude and time-radius diagrams of the azimuthally averaged azimuthal component of the magnetic field are shown in panels D and E. On these panels the magnetic cycle clearly appears. The most rotationally constrained model (Figure 4) remains in a very stable symmetric state about the equator, while the two other cases exhibit a clear beating between the quadrupolar (symmetric) and dipolar (anti-symmetric) modes of the large-scale dynamo. The convective luminosity profile throughout the convection zone is shown in panel F. It greatly varies with radius due to the convection-forcing scheme[42]. We choose to define the convective luminosity of our models by averaging it over the gray band in panel F, which is were the oscillatory dynamo primarily resides. Finally, the Fourier spectrum at depth $r=0.75\ R_\star$ and latitude 44° is shown in panel G. A peak is identified clearly for each case. The cycle period reported in this work (see Figures 2 and 3) are defined based on the whole domain time-evolution, and is calculated as follows.

Estimation of the cycle period. We estimate the magnetic cycle period in our numerical simulations by running a Fourier transform on the longitudinally averaged azimuthal component of the magnetic field at all points in radius and latitude. The main peak of the Fourier transform (see panel G in Figures 4-6) is stored at each point, along with a period bandwidth defined as a band around the main peak for which the Fourier transform is larger than 10% of its peak value. A probability density function is formed with all the stored peaks, and the maximum of the distribution defines the main cycle period of the simulation. The error-bar on the cycle period is taken as the maximal bandwidth associated with the cycle-period. Note that the cycle period in Figure 2 is actually the half-cycle period (*i.e.* 11 years for the Sun).

Estimation of the convective luminosity. The convective luminosity is estimated by computing the azimuthal and latitudinal average of the convective heat flux averaged over several cycle periods such as

$$L(r) = 4\pi r^2 \rho c_p < v_r T' >,$$

where T' are the temperature fluctuation, v_r the radial velocity, ρ the density, c_p the specific heat of the plasma at constant pressure, and <> stands for average over the spherical of radius *r* and over time (over several magnetic cycles). The convective luminosity at the base of the convection zone L_{bc} is defined here as the average of the convective luminosity L over the $[0.75\ R_\odot, 0.8\ R_\odot]$ radial interval (see panel F in Figures 4-6), in the region where dynamo action is taking place and safely away from the lower boundary.

Estimation of the Rossby number. The Rossby number quantifies the relative importance of non-linear advection to the Coriolis acceleration in the Navier-Stokes equation of fluid dynamics expressed in a rotating frame of reference. In the context of cool stars, it is often also defined as a ratio of two timescales, the rotation period of the star, and the convective turnover time at the base of the convection zone of the star. In this work we calculate the Rossby number as

$$R_o = | \nabla \times \mathbf{u} | / (2 \Omega_\star),$$

which is the ratio of vorticity of the convective flows over the rotation rate of the star. The Rossby number is averaged over time and longitude, over the same radial range $[0.75\ R_\odot, 0.8\ R_\odot]$ as the convective luminosity, and over a latitudinal wedge of 140° centered on the equator. The error-bar on the Rossby number is set with its standard deviation over the averaging surface in the radius-latitude plane.

Estimation of the luminosity of the observed stars. We follow the standard procedure[29] to estimate the luminosity of a star in the two samples used in this study. The effective temperatures of the stars were originally published along the reported cycle periods[5,27]. The luminosity $L_\star$ of a star can be approximated through

$$\mathrm{Log}_{10} (L_\star / L_\odot) = -0.4 (m_V - 5\ \mathrm{Log}_{10}(d/10) + BC_V - M_{bol}^{\odot}) ,$$

where m_V is the apparent magnitude in V band, d the distance between the Sun and the star (in parsec), $M_{bol}{}^{\odot}$ the bolometric magnitude of the Sun and BC_V the so-called bolometric correction, which is an empirical function the effective temperature[29]. The distance d and m_V were taken from the latest Hipparcos catalogue[28]. A sub-sample of the stars analyzed here is also present in the Gaia catalogue[43]. We re-derived the stellar luminosities with the Gaia parallaxes and did not find a significant change in the results presented in this work.

Re-analysis of the cycle periods in the L11 sample[27]. The observational evidence for an activity cycle on distant stars is tedious to obtain, as it requires a long-term monitoring over a decadal time-scale. The HARPS spectrograph has monitored a few hundred stars since 2003, and can thus be used to probe for activity cycles of a few years in distant stars[27]. These results were nonetheless never fully published, due in part to the large uncertainties on the reported activity cycle periods in this large sample of stars. In this work we reported the complete initial sample[27] as transparent diamonds in Figure 2, for reference. A major result from the HARPS data was the existence of stars with magnetic cycles populating the (P_{rot}, P_{cyc}) diagram in between the two historically determined branches of activity, where the Sun was before lying alone as an anomalous (or in-transition) solar-type star. In this work we re-analyzed these particular stars of the HARPS sample to identify the robustness of the reported activity cycle periods (plain orange diamonds in Figure 2). We show in Figure 7 one of these stars, HD 146233 (also known as 18 Sco) which one of the closest solar-twin discovered yet[44]. A solar twin has fundamental physical parameters very similar, if not identical, to those of the Sun[45]. 18 Sco is a bright star (V = 5,49) G-type stars within 50 parsecs of the Sun. We observe that its folded activity index indeed exhibit a cyclic pattern of about 7 years. In addition, the independent monitoring at Lowell Observatory (*J. Hall, personal communication*) also corroborates this cyclic activity of 18 Sco. All the 8 stars shown as orange diamonds in Figure 2 present an unambiguous periodicity in their Ca II R'_{HK} index, albeit with somewhat large error-bars, which gives us confidence in their inclusion along the historical data-set of the Mt Wilson observatory[5]. A careful re-analysis of the remaining sample[27] still remains to be done, and may require longer-term observations that will be available in the future.

References

J'ajouterais ici les ref. qui ne sont que dans les annexes à la fin, quand on aura convergé définitivement sur le texte.

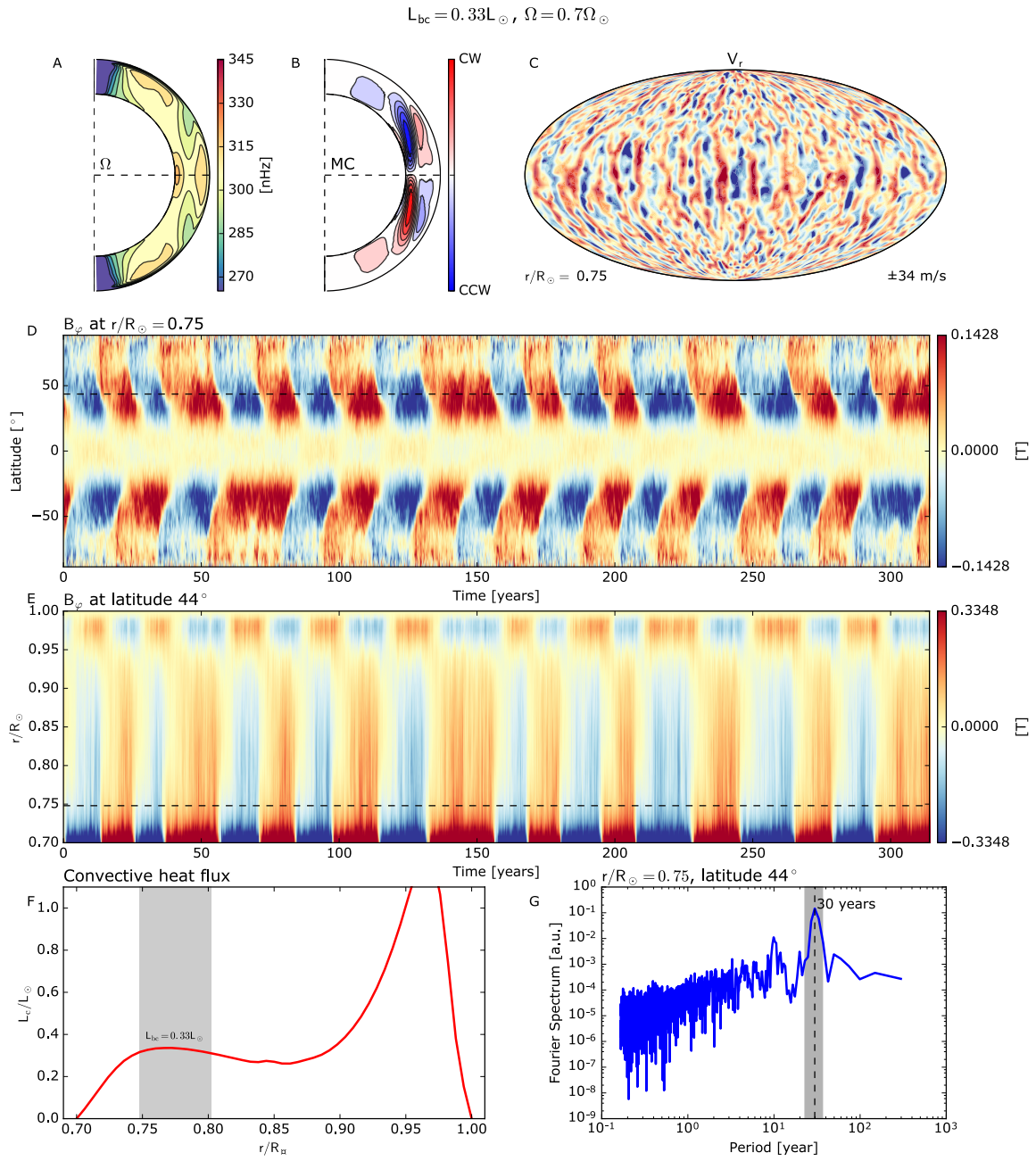

Figure 4 | Reference case (A) Differential rotation profile averaged over time and longitude. (B) Meridional circulation contours averaged over time and longitude. Clock-wise circulations are shown in red, anti-clockwise in blue. (C) Radial velocity on a Mollweide projection on the sphere at depth r=0.75 $R_\star$. Red denotes upflows and blue downflows. (D) Azimuthal component of the magnetic field averaged over longitude as a function of time and latitude at depth r=0.75 $R_\star$ (near the base of the convection zone). (E) Azimuthal component of the magnetic field averaged over longitude as a function of time and normalized radius at latitude 44°. (F) Convective luminosity (see Methods section) as a function of depth. The grey band corresponds to the depth of large magnetic fields where we choose to estimate the convective luminosity used in Figure 2. (G) Fourier spectrum of the azimuthal component of the magnetic field at depth r=0.75 $R_\star$ and latitude 44° (dashed black lines in panels D and E). The peak of the spectrum shows the magnetic cycle period. The magnetic cycle periods shown in Figure 2 and 3 are calculated with Fourier spectra on the

whole (r,latitude) domain (see Methods section). The vertical grey bar shows the uncertainty on the cycle period based on the Fourier spectrum.

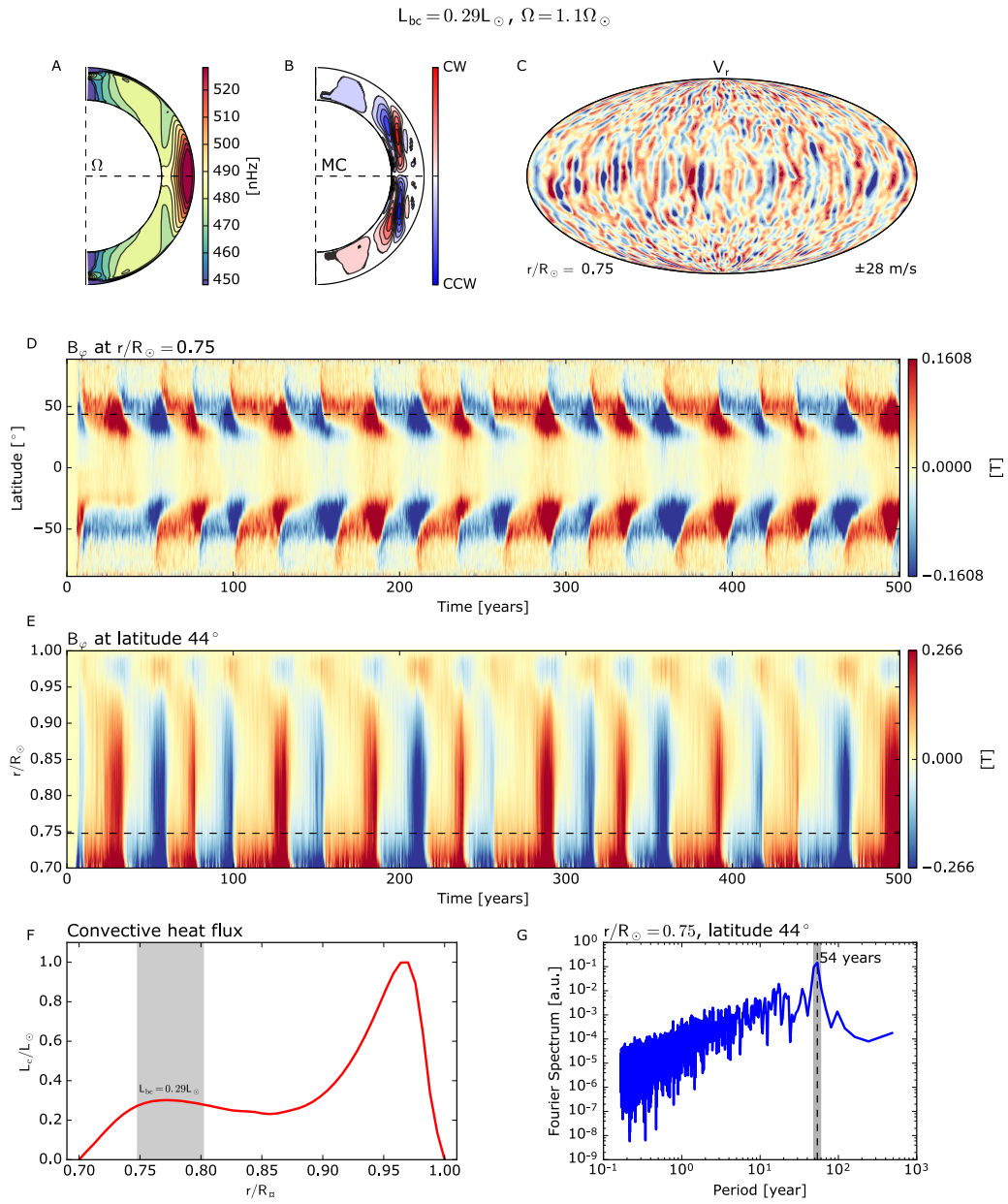

Figure 5 | Larger rotation case The layout is the same as in Figure 4.

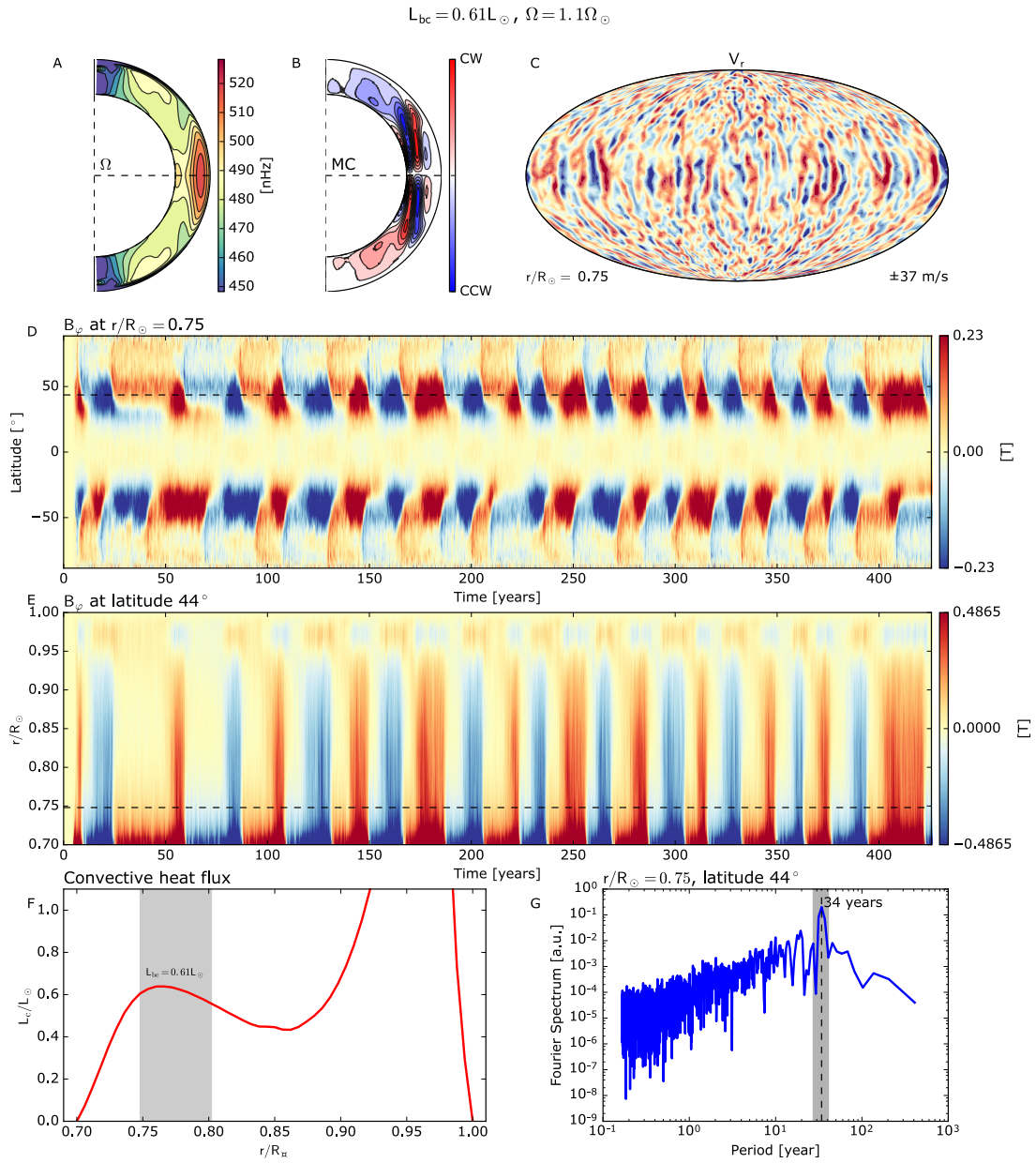

Figure 6 | Larger rotation and luminosity case The layout is the same as in Figure 4.

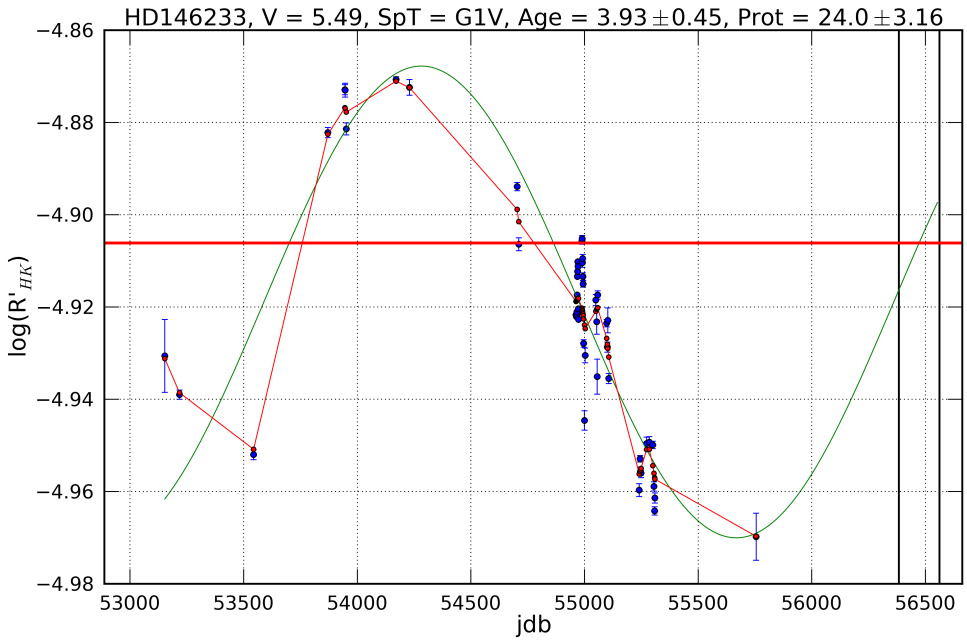

Figure 7 | Activity cycle in HD146233 HD 146233 (18 Scorpii; HR 6060), is one of the stars identified as a "Solar twin". Its R'_{HK} from the HARPS data (blue points with error-bars) is shown folded on the reported activity period of about 7 years (green curve).